Debonding in FRP strengthened beams: stress assessment versus fracture mechanics approach

A. Carpinteri, P. Cornetti & N. Pugno
Dipartimento di Ingegneria Strutturale e Geotecnica, Politecnico di Torino, Turin, Italy

ABSTRACT: In the present paper we analyze the debonding failure of a beam strengthened by a fiber reinforced polymer. We propose an analytical approach, whose basic assumptions are that (i) sections inside the beam remain plane and (ii) the adhesive layer acts as a shear lag. A stress concentration is found at the edge of the reinforcement length. Two failure criteria are proposed to study the debonding process. The former is a stress assessment criterion, i.e. failure takes place whenever the maximum tangential stress reaches a limit value (the interfacial bond strength). The latter is an energy, fracture mechanics criterion, i.e. failure takes place as long as the strain energy release rate due to debonding reaches a critical value (the interfacial fracture energy). By means of Castigliano's theorem, the load vs. deflection graph is drawn, showing the possible rising of both snap-back and snap-through instabilities.

1 INTRODUCTION

One of the most promising techniques for strengthening existing structures is the use of strips made of fibre-reinforced polymers (FRP), bonded to the tensile side of the structure. The advantages of this technique are different. FRP strips are easy to install and cause a minimum increase in dimension; furthermore, they have a high strength, a light weight and a long durability.

The behaviour of the strengthened members is substantially different from that of the original structures. Referring to concrete beams, the FRP retrofitting causes a reduced ductility, a different shear response and, more importantly, different failure modes. Among the various failure modes observed, a special interest has been devoted to the debonding of the FRP because of its brittle and catastrophic features, the propagation of the interfacial crack being highly unstable.

In order to predict the critical load at which the debonding phenomenon takes place, several models have been proposed to evaluate the interfacial stresses. They all focus onto the prediction of the stresses in the vicinity of the edge of the FRP strip. These stresses are then used to predict the peak load. A critical review of these models can be found in the paper by Muckopadhyaya & Swamy (2001); the paper concludes that the existing models are too complex for use in practical design.

However, because of the brittleness of the debonding process, an energy approach seems to be more effective, since stress-based failure criteria are more suitable for gradual and ductile failures. An energy-based fracture criterion has recently been proposed by Rabinovitch (2004) and, later, by Colombi (2006), by applying the linear elastic fracture mechanics (LEFM) concept of energy release rate. In other words, the debonding process is assumed to begin when the energy release due to an infinitesimal crack growth is equal or higher than a critical value, i.e. the interfacial fracture energy. The aforementioned papers show that simplified models assuming a constant stress field across the adhesive layer thickness can be used to predict the energy release rate. However, its (approximate) evaluation is performed numerically by comparing the energetic state of the whole structure before and after a small interfacial crack growth.

A similar approach, applied to analyse delamination in a different geometry, has been recently proposed by Andrews et al. (2006). Moreover, among recent works based on neighbouring arguments, we cite the papers by Greco et al. (2007) for the evaluation of the strain energy release rate and the paper by Ferracuti et al. (2006) on numerical approaches to FRP debonding.

Aim of the present paper is to introduce a model to analyse FRP strengthened beams. The main simplifying assumption is that the adhesive layer acts as a *shear lag*, i.e. only shear stresses constant over its thickness are considered (for other applications of the shear lag model see, for instance, Stang et al., 1990; Pugno & Carpinteri, 2003). The model is

similar to others already available in the literature (Vilnay, 1988; Triantafillou & Deskovic, 1991; Taljsten, 1997; Malek et al., 1998; Smith & Teng, 2001, and references herein). The stress field provided by the model is used to apply the LEFM criterion. With respect to the papers by Rabinovitch (2004) and Colombi (2006), the novelty is that an analytical expression for the energy release rate is provided. It is believed that this can be useful for including debonding failure assessment in practical design codes. Furthermore, the present analytical approach allows one to obtain the complete load vs. displacement diagram, highlighting the possible rising of snap-back and snap-through instabilities (Carpinteri 1984; Carpinteri 1989a, b).

2 EQUIVALENT BEAM MODEL

The easiest analytical model to handle beams strengthened by FRP is the so-called equivalent beam model, based on the assumption of a planar cross section for the whole structure. Let us refer to a beam with a rectangular cross section (Fig. 1), whose width is t. In the following, the quantities with subscript b refer to the beam to be strengthened, the quantities with subscript a refer to the adhesive layer and the ones with subscript r to the reinforcement. Thus E_b, E_r, G_a are the Young moduli of the beam, of the reinforcement and the shear modulus of the adhesive; h_b, h_r, h_a are their respective thicknesses. In order to achieve a dimensionless formulation of the problem, it is convenient to normalise all the quantities with respect to the beam ones, i.e.:

$$n_a = \frac{G_a}{E_b}, \ n_r = \frac{E_r}{E_b}, \ \delta_a = \frac{h_a}{h_b}, \ \delta_r = \frac{h_r}{h_b}, \ \mu = \frac{t}{h_b} \quad (1)$$

For the sake of simplicity, it is convenient to introduce also the mechanical percentage of reinforcement:

$$\rho = \frac{E_r}{E_b} \frac{h_r}{h_b} = n_r \delta_r \quad (2)$$

Wishing to get analytical expressions as simple as possible, we can neglect the heights of the adhesive and of the reinforcement with respect to the beam height as well as the contribution of the adhesive layer to the moment of inertia. Thus, with respect to the bottom of the strengthened beam, the position y_G of the centre of gravity of the whole section is (Fig. 1):

$$y_G = \frac{h_b}{2(1+\rho)} \quad (3)$$
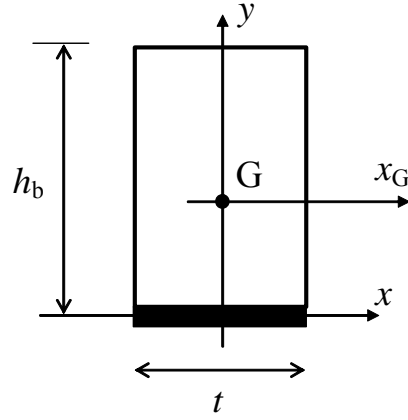
Figure 1. Geometry of the reinforced cross section.

The moment of inertia with respect to the x_G axis reads:

$$I = \frac{1+4\rho}{1+\rho} I_b \quad (4)$$

$I_b = t \, h_b^3 \, / \, 12$ being the moment of inertia of the plain beam section.

Let us consider a three point bending geometry (Fig. 2). The beam span is $2l$ and P is the concentrated load. If z is the axial coordinate with origin at the beam mid-span, in the left side of the beam the shear force is $T = P/2$ and the bending moment is $M = - P \, (l-z) \, /2$. Therefore, according to the well-known equivalent beam model, the horizontal normal stress σ_r in the reinforcement and the shear stress τ_a in the adhesive layer are, in dimensionless form:

$$\frac{\sigma_r}{E_b} = \frac{3n_r}{1+4\rho} \frac{\Pi \lambda}{\mu} (1-\zeta), \ \ 0 < \zeta < \zeta_r \quad (5)$$

$$\frac{\tau_a}{E_b} = \frac{3\rho}{1+4\rho} \frac{\Pi}{\mu}, \ \ 0 < \zeta < \zeta_r \quad (6)$$

where Π, ζ, λ are respectively the dimensionless load, axial coordinate and length (i.e. the slenderness):
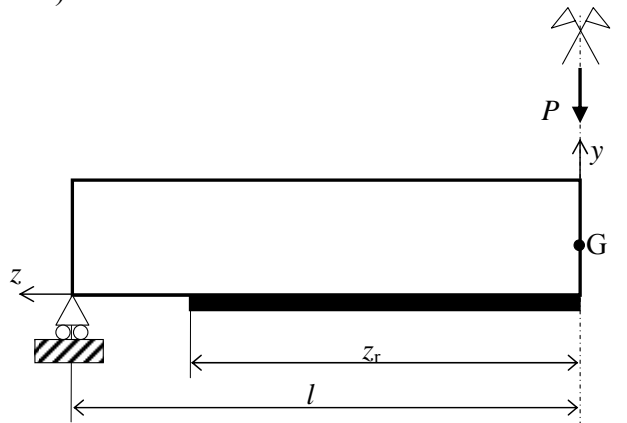
Figure 2. A FRP reinforced beam under three point bending flexural load. Symmetry is exploited to study only half of the structure.

$$\Pi = \frac{P}{E_b h_b^2} \,, \quad \zeta = \frac{z}{l} \,, \quad \lambda = \frac{l}{h_b} \tag{7}$$

The previous expressions are valid for the reinforced zone ($0 < \zeta < \zeta_r = z_r/l$); outside they vanish and the simple beam theory holds.

3 SHEAR LAG MODEL

With respect to the equivalent beam, a more refined model can be achieved by assuming that the cross sections remain planar after deformation only inside the beam to be strengthened. In fact it is argued that, since the main duty of the adhesive layer is to transfer stresses from the beam to the FRP reinforcement by means of tangential stresses, the shear stress and strain inside the adhesive layer have to be explicitly taken into account to have a more accurate description of the geometry analyzed.

In the following it is assumed that the adhesive layer acts as a shear lag, i.e. no normal stresses are considered within its thickness. Although more complex models can be set by considering also the normal stresses or describing the adhesive layer as a 2D medium, it is argued that the shear lag model could be a reasonable compromise for the description of the FRP debonding. The goal of the present paper is in fact to provide a model that is accurate enough to describe the basic features of the process and, at the same time, simple enough to be handled analytically.

The assumption of planar cross sections reads:

$$w_b(y,z) = w_{b0}(z) + \varphi_b(z)\, y \tag{8}$$

where w_b is the axial displacement of the beam points, φ is the rotation of the cross section at the distance z from the midspan and w_{b0} is the axial displacement of the points at the bottom of the beam. Denoting by ε_b and ε_r the dilations of the beam points and of the reinforcement and by γ_a the shearing strain of the adhesive, the assumption of a linear elastic behaviour for all the materials composing the structure yields:

$$\sigma_b = E_b \varepsilon_b = E_b\left(\frac{dw_{b0}}{dz} + \frac{d\varphi_b}{dz}\, y\right) = E_b(\varepsilon_{b0} + \chi_b\, y) \tag{9}$$

$$\tau_a = G_a\, \gamma_a = G_a \frac{w_{b0} - w_r}{h_a} \tag{10}$$

$$\sigma_r = E_r\, \varepsilon_r = E_r \frac{dw_r}{dz} \tag{11}$$

where χ_b is the beam curvature.

The problem can now be solved by imposing the equilibrium. The first two solving equations state the equivalence of the stress distribution with the axial force (which is equal to zero) and with the bending moment M; the third one represents the differential equilibrium of the reinforcement along z:

$$\int_0^{h_b} \sigma_b\, t\, dy + \sigma_r\, t\, h_r = 0 \tag{12}$$

$$\int_0^{h_b} \sigma_b\, y\, t\, dy = M \tag{13}$$

$$h_r \frac{d\sigma_r}{dz} + \tau_a = 0 \tag{14}$$

By substitution of eqns(9-11) into eqns(12-14) and by a further derivation of the last equation, we get:

$$\begin{cases} \varepsilon_{b0} + \dfrac{h_b}{2}\chi_b + \rho\varepsilon_r = 0 \\[2mm] \dfrac{1}{2}\varepsilon_{b0} + \dfrac{h_b}{3}\chi_b = -\dfrac{P}{2th_b^2 E_b}(l-z) \\[2mm] \dfrac{d^2\varepsilon_r}{dz^2} - \dfrac{G_a}{E_r h_r h_a}(\varepsilon_r - \varepsilon_{b0}) = 0 \end{cases} \tag{15}$$

This is a system of three equations, the first two algebraic and the last one differential. The three unknowns are the deformation functions $\varepsilon_{b0}(z)$, $\chi_b(z)$ and $\varepsilon_r(z)$. By substitution, it is possible to obtain a differential equation, which, in dimensionless form, reads:

$$\frac{d^2\varepsilon_r}{d\zeta^2} - \beta^2\varepsilon_r = -\frac{3\beta^2}{1+4\rho}\frac{\Pi\lambda}{\mu}(1-\zeta) \tag{16}$$

where:

$$\beta^2 = \frac{G_a l^2}{E_r h_r h_a}(1+4\rho) = \frac{1+4\rho}{\rho}\frac{n_a}{\delta_a}\lambda^2 \tag{17}$$

Before solving the differential equation (16), it is interesting to observe that, if the thickness of the adhesive layer tends to zero (i.e. $\beta^2 \to \infty$), the solution tends to the one of the equivalent beam model (i.e. eqn (5)):

$$\varepsilon_r = \frac{3}{1+4\rho}\frac{\Pi\lambda}{\mu}(1-\zeta) \tag{18}$$

except in the neighbourhood of the end of the reinforcement where the second derivative of ε_r is unbounded. Furthermore, it can be easily verified that the equivalent beam solution (18) is a particular integral of the differential equation. As well known, the complete solution is given by the sum of a particular integral and the solution of the associated homogeneous equation. Thus:

$$\varepsilon_r = A\,e^{+\beta\zeta} + B\,e^{-\beta\zeta} + \frac{3}{1+4\rho}\frac{\Pi\lambda}{\mu}(1-\zeta) \qquad (19)$$

In order to determine the constants A and B, two boundary conditions are needed. The first one derives from symmetry considerations, whereas the second one implies a zero normal stress in the FRP at the edge of the reinforced zone:

$$\frac{d\varepsilon_r}{d\zeta} = 0, \quad \text{if } \zeta = 0 \qquad (20a)$$

$$\varepsilon_r = 0, \quad \text{if } \zeta = \zeta_r \qquad (20b)$$

It is interesting to note that both the conditions are violated by the equivalent beam model, where the stress at the edge of the FRP is different from zero and the strain at mid-span is not differentiable.

Observe that, at mid-span, one can also set the strain in the reinforcement equal to the value provided by the equivalent beam model. However the effect of the boundary condition at $\zeta = 0$ has a negligible effect at the FRP strip edge ($\zeta = \zeta_r$). See Smith & Teng (2001) for a discussion about this point.

By means of the boundary conditions, the final solution is:

$$\varepsilon_r = \frac{3}{1+4\rho}\frac{\Pi\lambda}{\mu}f_\varepsilon \qquad (21a)$$

with:

$$f_\varepsilon = (1-\zeta) - \frac{\beta(1-\zeta_r)\cosh(\beta\,\zeta) + \sinh[\beta(\,\zeta_r - \zeta)]}{\beta\,\cosh(\beta\,\zeta_r)} \qquad (21b)$$

Function $f_\varepsilon = f_\varepsilon(\zeta,\zeta_r,\beta)$ has been introduced for the sake of simplicity: in fact it is possible to express all the quantities as functions of f_ε and its derivatives and integrals. Through eqns (11) and (14), the horizontal normal stress and the shear stress respectively in the FRP and in the adhesive layer read:

$$\frac{\sigma_r}{E_b} = \frac{3n_r}{1+4\rho}\frac{\Pi\lambda}{\mu}f_\varepsilon \qquad (22)$$

$$\frac{\tau_a}{E_b} = -\frac{3\rho}{1+4\rho}\frac{\Pi}{\mu}\frac{\partial f_\varepsilon}{\partial\zeta} = \frac{3\rho}{(1+4\rho)}\frac{\Pi}{\mu} \times$$
$$\times \left\{1 + \frac{\beta(1-\zeta_r)\sinh(\beta\,\zeta) - \cosh[\beta(\,\zeta_r - \zeta)]}{\cosh(\beta\,\zeta_r)}\right\} \qquad (23)$$

while, from the system (15), the beam curvature is:

$$\chi_b h_b = 6\left[\rho\varepsilon_r - \frac{\Pi\lambda}{\mu}(1-\zeta)\right] = \frac{6\Pi\lambda}{\mu}\left[\frac{3\rho}{1+4\rho}f_\varepsilon - (1-\zeta)\right] \qquad (24)$$
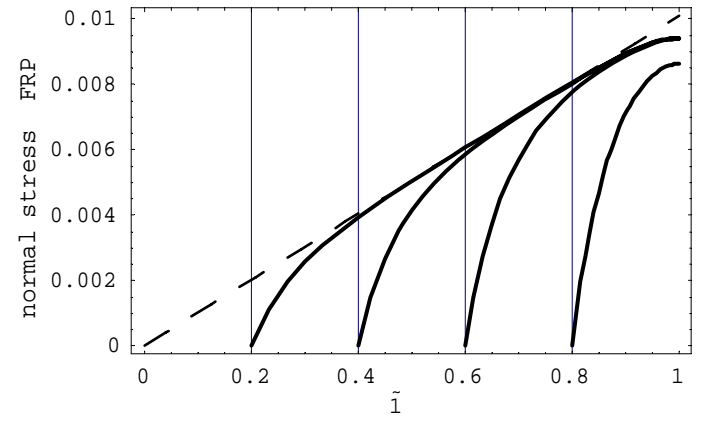
Figure 3. Horizontal normal stress in the FRP versus the axial coordinate (dimensionless quantities). The thick lines refer to a bonded length ζ_r equal to 0.8, 0.6, 0.4, 0.2 from right to left. The dashed line represents the equivalent beam model solution.
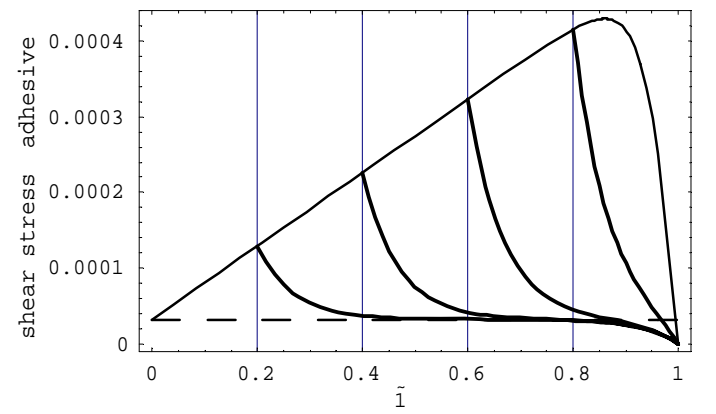
Figure 4. Shear stress in the adhesive layer versus the axial coordinate (dimensionless quantities). The thick lines refer to a bonded length ζ_r equal to 0.8, 0.6, 0.4, 0.2 from right to left. The dashed line represents the equivalent beam model solution. The thin line is the envelope of the maximum values of the shear stress.

In order to have a preliminary check of the capabilities of the model, the main quantities are now plotted with reference to an FRP-strengthened concrete beam. However it should be observed that, when considering a concrete beam to be retrofitted, the results of the present model are essentially indicative since: (i) the contribution of the concrete external cover to the interface compliance cannot be neglected with respect to the contribution of the adhesive layer; (ii) concrete cracking is expected to take place after debonding, whereas in the present model the material is assumed to be linear elastic throughout the debonding process.

Keeping in mind these restrictions, the stress fields (22) and (23) are plotted in Figs. 3 and 4 for different bonded lengths ζ_r and for the following material and geometric properties: $t = 100$ mm, $l = 500$ mm; $h_b = 120$ mm, $h_a = 4$ mm, $h_r = 1.6$ mm; $E_b = 30$ GPa, $G_a = 0.72$ GPa, $E_r = 160$ GPa; $P = 70$ kN. The dashed lines represent the equivalent beam model solution, which is independent of ζ_r. It is evident that, with respect to the simpler beam model, the shear lag model is able to catch the shear stress

concentration at the edge of the FRP strip, which is the cause of the FRP debonding. On the other hand, beyond a certain distance from the mid-span and the edge of the reinforcement, the two solutions coincide. More in detail, it can be proved that, for h_a tending to zero, the shear lag solution shows a non-uniform convergence to the equivalent beam solution.

4 FAILURE STRESS CRITERION

The maximum value of the shearing stress in the adhesive layer is attained at the end of the reinforced zone, i.e. for $\zeta = \zeta_r$:

$$\frac{(\tau_a)_{max}}{E_b} = \frac{3\rho}{(1+4\rho)} \frac{\Pi}{\mu} \left[1 + \frac{\beta(1-\zeta_r)\sinh(\beta\,\zeta_r) - 1}{\cosh(\beta\,\zeta_r)} \right] (25)$$

Introducing the shearing strength τ_p, the dimensionless load Π_c causing debonding is therefore:

$$\Pi_c = \frac{(1+4\rho)\mu}{3\rho} \frac{\tau_p}{E_b} \frac{\cosh(\beta\,\zeta_r)}{\cosh(\beta\,\zeta_r) + \beta(1-\zeta_r)\sinh(\beta\,\zeta_r) - 1} \tag{26}$$

For the geometry given above, the critical load vs. reinforced zone length is plotted in Figure 5 for a τ_p value equal to 5 MPa. Since the debonded portion of the FRP strip becomes stress free, the plot in Figure 5 can be interpreted as either the graph of the critical loads for different initial lengths of the FRP strip, or the diagram of the load during the debonding process for a given initial FRP strip length. In the latter case, it is interesting to observe that, if the process is load-controlled, the debonding process is unstable until the reinforcement length is much shorter than the beam length (about 20%). Then, an increase in the load is required to have a further debonding; however the strengthening effect of the FRP is rather negligible at that stage.
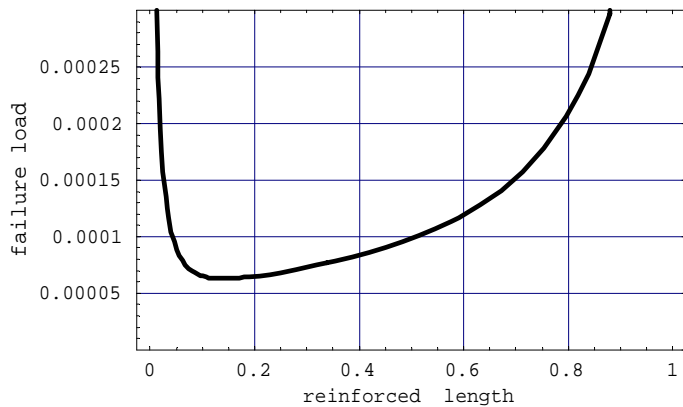
Figure 5. Failure load versus reinforced length ζ_r according to the stress-based failure criterion (dimensionless quantities).

About the validity of the stress criterion (26), a first drawback is that, for h_a tending to zero, the maximum tangential stress tends to infinity and the critical load vanishes, a result which is physically meaningless. Furthermore, finite element analyses show that, at the edges of the FRP strip, in addition to shear stresses, localized vertical normal stresses (along y) are present which are not caught by the present model. Neglecting this local effect could affect the predictive capability of the stress-based failure criterion (26). For these reasons, in the following section a fracture energy criterion, based on LEFM, is put forward. As a matter of fact, it is argued that the energy criterion should be more reliable with respect to the local stress failure criterion since it is based on an overall energy balance. The brittleness of the debonding phenomenon justifies the use of LEFM. Finally, it will be shown that the energy criterion provides a finite failure load for an adhesive layer thickness tending to zero.

5 FRACTURE ENERGY CRITERION AND RELATED SNAP-BACK AND SNAP-THROUGH INSTABILITIES

The computation of the strain energy Φ must be divided in the sum of four terms, i.e. the strain energy within the FRP strip (Φ_r), the adhesive layer (Φ_a), the portion of the beam above the FRP (Φ_{b1}) and the one where there is no reinforcement (Φ_{b2}). The first, the second and the fourth contributions are straightforward:

$$\Phi_r = \frac{h_r}{2E_r} \int_0^{z_r} \sigma_r^2 \, dz \tag{27a}$$

$$\Phi_a = \frac{h_a}{2G_a} \int_0^{z_r} \tau_a^2 \, dz \tag{27b}$$

$$\Phi_{b2} = \frac{1}{2} \int_{z_r}^{l} \frac{M^2}{E_b I_b} \, dz \tag{27c}$$

About the third contribution (Φ_{b1}), it should be noted that, by marking with ε_{bG} the axial dilation of the centre of gravity of the cross section (without the reinforcement, i.e. $y = h/2$), the classical beam theory yields:

$$\Phi_{b1} = \frac{E_b A_b}{2} \int_0^{z_r} \varepsilon_{bG}^2 \, dz + \frac{E_b I_b}{2} \int_0^{z_r} \chi_b^2 \, dz \tag{27d}$$

where $A_b = t\, h_b$. Since the axial force is zero, $\varepsilon_{bG} = \rho\varepsilon_r$. Skipping analytical computations, the strain energy of the whole structure can be expressed in di-

mensionless form ($\tilde{\Phi} = \Phi / E_b h_b^3$) by means of eqns (21-24):

$$\tilde{\Phi} = \frac{\lambda^3 \Pi^2}{2\mu}\left[1 + \frac{9\rho}{1+4\rho}F(\zeta_r,\beta)\right] \qquad (28)$$

where:

$$F(\zeta_r,\beta) = \int_0^{\zeta_r}\left\{f_\varepsilon[f_\varepsilon - 2(1-\zeta)] + \frac{1}{\beta^2}\left(\frac{\partial f_\varepsilon}{\partial \zeta}\right)^2\right\}d\zeta \qquad (29)$$

Function F can be computed analytically; nevertheless, since its expression is rather long, we prefer to omit it. Details will be given elsewhere. Let us observe that the unit term within square brackets in eqn (28) represents the strain energy when no reinforcement is present; hence it is clear that function F is always negative, except for $\zeta_r = 0$, when it is equal to zero.

Once the strain energy is obtained, the energy release rate is provided by deriving the previous expression with respect to the interfacial crack length a. Since $da = -d\zeta_r$, we have:

$$G = -\frac{1}{t}\frac{d\Phi}{dz_r} \qquad (30)$$

We assume a symmetrical debonding growth with respect to the mid-span. In dimensionless form ($g = G/E_b h_b$):

$$g = -\frac{1}{\lambda\mu}\frac{d\tilde{\Phi}}{d\zeta_r} = -\frac{9\lambda^2\Pi^2}{2\mu^2}\frac{\rho}{1+4\rho}F'(\zeta_r,\beta) \qquad (31)$$

where the prime denotes derivative with respect to ζ_r. Observe that, since F' is negative, g is always positive, as we should have expected.

According to LEFM, the energy criterion states that debonding starts whenever the energy release rate reaches its critical value G_c (called also fracture energy): $G = G_c$. The dimensionless critical load Π_c is therefore given by ($g_c = G_c / E_b h_b$):
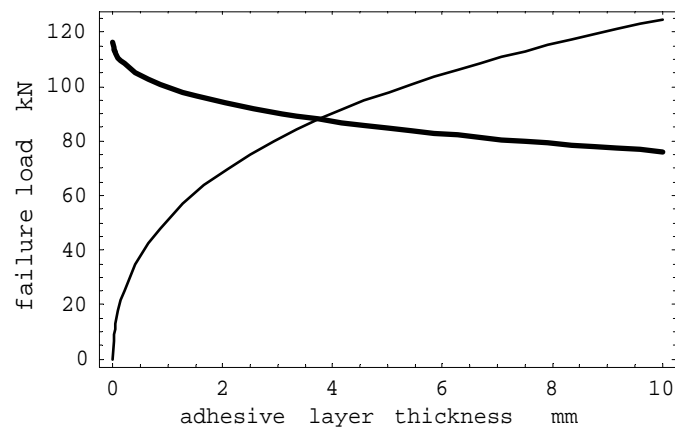
Figure 6. Failure load versus adhesive layer thickness according to the stress criterion (thin line) and to the energy criterion (thick line) for $\zeta_r = 0.8$, $\tau_p = 5$ MPa, $G_c = 65$ J/m^2; the values of the other parameters are given in the text.

$$\Pi_c = \frac{\mu}{3\lambda}\sqrt{-\frac{2(1+4\rho)g_c}{\rho F'(\zeta_r,\beta)}} \qquad (32)$$

Hence, according to the present LEFM criterion, no FRP debonding is expected if:

$$\Pi < \Pi_c \qquad (33)$$

Qualitatively, the plot of the critical load Π_c vs. ζ_r provided by the energy criterion is similar to the previous one provided by the stress criterion (26): the difference is mainly due to the different values of the parameter governing failure (G_c instead of τ_p). However, the effect of the adhesive layer thickness is opposite: as shown in Figure 6, according to the energy approach, the failure load usually decreases increasing the thickness, while it increases according to the stress approach. More in detail, while the critical value (26) vanishes for a null adhesive thickness, the critical value (32) tends to a constant (i.e. the same value provided by the equivalent beam model). It is argued that the failure load is the highest among the two predictions, since both energy and stress requirements have to be fulfilled to trigger the debonding process. It is worth noting that, if more failure mechanisms are present (e.g. brittle fracture and plastic collapse) the critical mechanism is the one providing the lowest failure load. However this is not the present case, since the stress criterion (26) is a *local* brittle fracture criterion, i.e. it does *not* coincide with the plastic collapse.

From a practical point of view, in order to be effective, the FRP strip must be glued by a sufficiently thin adhesive layer, i.e. usually the adhesive thickness is such that the energy criterion prevails.

Since the energy release rate provided by the equivalent beam model coincides with the value provided by the shear lag model with a null adhesive thickness, Figure 6 shows also that, if the energy fracture criterion is to be used, the equivalent beam model, for the usual reinforcement lengths, provides an overestimate of the failure load if compared to the more refined shear lag model; therefore its application may be potentially dangerous.

Because of the above considerations (and the uncertainties related to the stress fields provided by the analytical models highlighted in the previous section), hereafter we make use only of the estimate of the failure load based on the fracture energy criterion (32).

In order to analyse the presence of snap-back and/or snap-through instabilities during the debonding process, the plot of the load P vs. the vertical displacement v at mid-span has to be sought. This can be easily achieved by means of Castigliano's theorem, since we already know the expression of the strain energy of the whole system. Therefore, the strain energy Φ must be derived with respect to the load P:

Table1. Comparison between analytical approaches and numerical simulations.

| | Energy release rate | Maximum shear stress | Mid-span displacement |
	J/m^2	MPa	mm
Shear lag model	41.83	3.880	2.832
Equivalent beam model	23.55	0.9689	2.820
Finite element analysis	Not available	3.266	2.818

$$v = 2\frac{d\Phi}{dP} \qquad (34)$$

where the coefficient 2 appears since Φ is the energy contained in half of the beam. In dimensionless form ($\eta = v/h_b$):

$$\eta = 2\frac{d\tilde{\Phi}}{d\Pi} = \frac{2\lambda^3\Pi}{\mu}\left[1 + \frac{9\rho}{1+4\rho}F(\zeta_r,\beta)\right] \qquad (35)$$

In order to have a preliminary check of the analytical results obtained so far, we performed also a finite element analysis of the three point bending geometry described above. In table 1, the numerical results are compared to the ones obtained through the equivalent beam model and the shear lag model. It is evident that the shear lag model shows results which are closer to the numerical simulations and, apart from the mid-span displacement, very different from the values provided by the equivalent beam model.

Substituting eqn (32) into eqn (35), we get the displacement at mid-span at the critical condition:

$$\eta = \frac{2\lambda^2}{3}\sqrt{-\frac{2(1+4\rho)g_c}{\rho F'(\zeta_r,\beta)}}\left[1 + \frac{9\rho}{1+4\rho}F(\zeta_r,\beta)\right] \qquad (36)$$

Eqns (32) and (36) can be seen as the equation of a curve in the plane (Π,η) defined parametrically by means of ζ_r. The curve Π vs. η is plotted in Figure 7 according to the geometrical and material data provided above; furthermore, a fracture energy $G_c = 65$ J/m^2 has been assumed, which corresponds to the concrete fracture energy, since the debonding crack typically runs under the concrete skin. For the sake of clarity, in Figure 7 also the straight lines corresponding to the beam configurations with a completely bonded FRP strip or without reinforcement have been drawn. It is seen that, if the plain beam does not collapse because of other failure mechanisms, the structural behaviour shows both snap-back and snap-through instabilities, i.e. function jumps if the process is displacement or load con-

trolled (Carpinteri 1984; Carpinteri 1989a, b). More in detail, the snap-back instability appears because of the positive slope of the softening branch in Figure 7. The snap-back appears to be rather severe, i.e. the critical load decreases considerably during the debonding process. In other words, the analytical results here presented clearly show that FRP debonding is a highly unstable and brittle phenomenon. Numerical simulations (Carpinteri et al., in press) seem to confirm the presence of snap-back instability detected by the present analytical approach.

6 CONCLUSIONS

In the present paper an analytical approach to study the debonding process of FRP strips from concrete beams has been addressed. The stress field provided by the model has been used to formulate a LEFM failure criterion. With respect to other approaches available in the literature, the present one has the advantage to be analytical: all the main quantities have been expressed as functions of dimensionless (geometrical and mechanical) parameters and of the analytical function f_ε (eqn (21b)). It is believed that these findings can be helpful for standard design codes requirements to avoid FRP debonding. Finally, the instabilities associated with the debonding process have been analyzed.
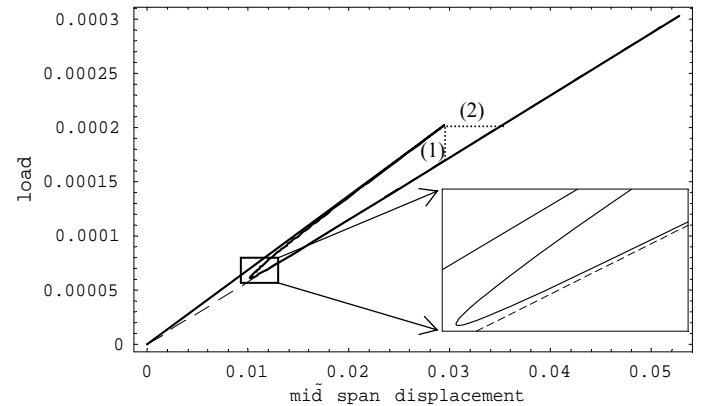
Figure 7. Load versus mid-span deflection (dimensionless quantities) for an initially bonded length ζ_r equal to 0.8. The dashed line represents the behaviour of a beam without reinforcement. The dotted lines represents snap-back (1) and snap-through (2) instabilities.

REFERENCES

Andrews, M.G., Massabò, R., Cox, B.N. 2006. Elastic interaction of multiple delaminations in plates subject to cylindrical bending. *International Journal of Solids and Structures*. 43:855-886.
Carpinteri, A., Lacidogna, G., Paggi, M. Acoustic emission monitoring and numerical modeling of FRP delamination in RC beams with non-rectangular cross-section. *RILEM Materials & Structures*, DOI 10.1617/s11527-006-9162-4.

Carpinteri, A. 1985. Interpretation of the Griffith instability as a bifurcation of the global equilibrium. In S.P. Shah (ed.), *Application of Fracture Mechanics to Cementitious Composites*: 287-316; *Proceedings of a NATO Advanced Research Workshop, Evanston, USA, 1984*. Dordrecht: Martinus Nijhoff Publishers.

Carpinteri, A. 1989a. Cusp catastrophe interpretation of fracture instability. *Journal of the Mechanics and Physics of Solids* 37:567-582.

Carpinteri, A. 1989b. Decrease of apparent tensile and bending strength with specimen size: two different explanations based on fracture mechanics. *International Journal of Solids and Structures* 25:407-429.

Colombi, P. 2006. Reinforcement delamination of metallic beams strengthened by FRP strips: Fracture mechanics based approach. *Engineering Fracture Mechanics* 73:1980-1995.

Ferracuti, B., Savoia, M., Mazzotti, C. 2006. A numerical model for FRP-concrete delamination. *Composites: Part B* 37: 356-364.

Greco, F., Lonetti, P., Nevone Blasi P. 2007. An analytical investigation of debonding problems in beams strengthened using composite plates. *Engineering Fracture Mechanics* 74:346-372.

Malek, A.M., Saadatmanesh, H., Ehsani, M.R. 1998. Prediction of failure load of R/C beams strengthened with FRP plate due to stress concentration at the plate end. *ACI Structural Journal* 95:142-52.

Muckopadhyaya, P. & Swamy, N. 2001. Interface shear stress: a new design criterion for plate debonding. *Journal of Composite Construction* 5:35-43.

Pugno, N. & Carpinteri A. 2003. Tubular adhesive joints under axial load. *Journal of Applied Mechanics* 70:832-839.

Rabinovitch, O. 2004. Fracture-mechanics failure criteria for RC beams strengthened with FRP strips – a simplified approach. *Composite Structures* 64:479-492.

Smith, S.T. & Teng, J.G. 2001. Interfacial stresses in plated beams. *Engineering Structures* 23, 857-871, 2001.

Stang, H., Li, Z., Shah, S.P. 1990. Pullout problem: stress versus fracture mechanical approach. *Journal of Engineering Mechanics* 116:2136-2150.

Taljsten, B. 1997. Strengthening of beams by plate bonding. *Journal of Materials in Civil Engineering, ASCE* 9:206-12.

Triantafillou, T.C. & Deskovic, N. 1991. Innovative prestressing with FRP sheets: Mechanics of short-term behavior. *Journal of Engineering Mechanics*. 117:1652-1672.

Vilnay, O. 1988. The analysis of reinforced concrete beams strengthened by epoxy bonded steel plates. *International Journal of Cement Composites and Lightweight Concrete*, 10:73-8.